JPE 19-1-18

https://doi.org/10.6113/JPE.2019.19.1.190
ISSN(Print): 1598-2092 / ISSN(Online): 2093-4718

Sampled-Data Modeling and Dynamic Behavior Analysis of Peak Current-Mode Controlled Flyback Converter with Ramp Compensation

Shuhan Zhou*, Guohua Zhou†, Shaohuan Zeng*, Shungang Xu*, and Taiqiang Cao**

†,*Key Laboratory of Magnetic Suspension Technology and Maglev Vehicle, Ministry of Education
School of Electrical Engineering, Southwest Jiaotong University, Chengdu, China
**School of Electrical Engineering and Electronic Information, Xihua University, Chengdu, China

Abstract

The flyback converter, which can be regarded as a nonlinear time-varying system, has complex dynamics and nonlinear behaviors. These phenomena can affect the stability of the converter. To simplify the modeling process and retain the information of the output capacitor branch, a special sampled-data model of a peak current-mode (PCM) controlled flyback converter is established in this paper. Based on this, its dynamic behaviors are analyzed, which provides guidance for designing the circuit parameters of the converter. With the critical stability boundary equation derived by a Jacobian matrix, the stable operation range with a varied output capacitor, proportional coefficient of error the amplifier, input voltage, reference voltage and slope of the compensation ramp of a PCM controlled flyback converter are investigated in detail. Research results show that the duty ratio should be less than 0.5 for a PCM controlled flyback converter without ramp compensation to operate in a stable state. The stability regions in the parameter space between the output capacitor and the proportional coefficient of the error amplifier are enlarged by increasing the input voltage or by decreasing the reference voltage. Furthermore, the ramp compensation also can extend to the stable region. Finally, time-domain simulations and experimental results are presented to verify the theoretical analysis results.

Key words: Flyback converter, Peak current-mode control, Ramp compensation, Sampled-data modeling, Stability boundary

I. INTRODUCTION

Switching DC-DC converters are strong nonlinear systems with rich nonlinear phenomena, including sub-harmonic oscillations [1], [2], period-doubling bifurcation [3], border-collision bifurcation [4], [5], chaos [6], [7] and so on. These nonlinear phenomena have large effects on the performances of switching DC-DC converters and have recently been extensively studied [4]-[9]. Studying and analyzing the mechanisms of the nonlinear behaviors in switching DC-DC converters is helpful to guide in the circuit parameters design [10], [11], which has a lot of theoretical significance and practical value in practical engineering applications.

The flyback converter, as a typical isolated converter, is widely used in small and medium-sized power situations due to its simplicity, low cost, good electrical isolation, and wide input-voltage range [12]-[14]. In particular, its topology includes a transformer, which makes it easy to obtain multiple output ports to supply the different levels of the output voltage [15], [16]. However, there is also a strong nonlinear phenomenon in flyback converters. Until now, there have only been a few research works dedicated to the nonlinear phenomena of flyback converters [17]-[20], which can be used to guide the design of the main circuit parameters. The output capacitor voltage-ripple is neglected in [17] and the output voltage is assumed as a constant. In this case, the system becomes one-dimensional. The dynamic behavior of a current-mode controlled flyback converter is studied by establishing a

Manuscript received Nov. 24, 2017; accepted Sep. 6, 2018
Recommended for publication by Associate Editor Il-Oun Lee.
†Corresponding Author: ghzhou-swjtu@163.com
Tel: +86-13982214343, Southwest Jiaotong University
*Key Lab. of Magnetic Suspension Technol. & Maglev Vehicle, Ministry of Education, School of Electr. Eng., Southwest Jiaotong Univ., China
**School of Electrical Eng. and Electron. Informat., Xihua Univ., China

one-dimensional discrete iterative map model. Nevertheless, it is unable to study dynamic behaviors with some parameters varying, such as the output capacitor and the proportional coefficient of the error amplifier in the output voltage feedback loop and so on. According to the state equation of the circuit, a precise three-dimensional discrete iterative map model of a flyback converter is obtained in [18]. Its stability and bifurcation characteristics are analyzed when the switching frequency and leakage inductance vary. A two-dimensional discrete iterative map model of a peak current-mode (PCM) controlled flyback converter is also obtained utilizing the state equation of the circuit [19], [20]. However, the modeling process and the discrete iterative map models based on the state equation are rather complicated, since it includes large computations, especially in solving the eigenvalue of a Jacobian matrix. Furthermore, these papers focus on dynamic behaviors when the main circuit parameters vary, such as the load resistor, inductor, input voltage and switching period. However, almost none of these works report the dynamic behaviors of flyback converters with variations of the control circuit parameters. Thus, it is still necessary to study the dynamic behaviors of the control circuit parameters and the output capacitor, in order to completely analyze their effects on the stability of a system.

In order to simplify the dynamic modeling and analysis, a sampled-data modeling method is performed to investigate the dynamics of a PCM controlled flyback converter with ramp compensation. The rest of this paper is organized as follows. In section II, the operation principle of the system and its sampled-data model are illustrated. Then the dynamic behaviors of a PCM controlled flyback converter with ramp compensation are analyzed via a bifurcation diagram and Lyapunov exponent spectrum in section III. In section IV, the stability boundary equations are obtained by solving the characteristic equation of a Jacobian matrix. Meanwhile, the operation-state regions are studied. Finally, section V presents time-domain waveforms and experimental results to visualize these nonlinear phenomena, followed by the conclusion in Section VI.

II. Sampled-Data Modeling of a PCM Controlled Flyback Converter With Ramp Compensation

A. PCM Controlled Flyback Converter with Ramp Compensation

Fig. 1(a) shows some schematics of a PCM controlled flyback converter utilizing ramp compensation, where the main circuit consists of the input voltage V_{in}, magnetic inductor L_m, ideal transformer with a turns ratio $N_P : N_S$, switch S_1, diode S_2, load resistor R and capacitor C with an equivalent series resistance R_C. The control circuit is made up of the sensing resistor R_s, a clock with a period T_s, RS-latch,

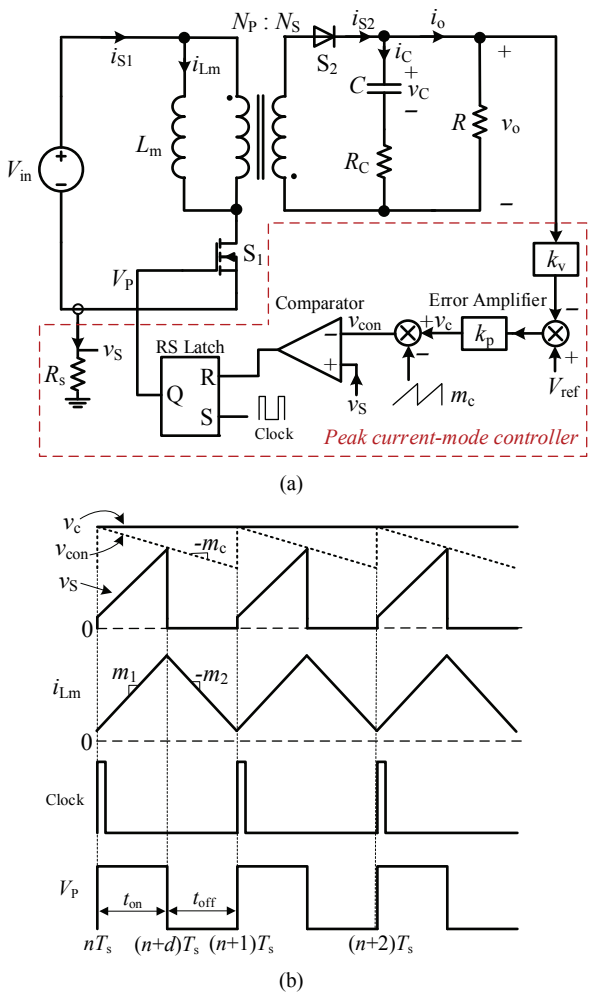

Fig. 1. PCM controlled flyback converter with ramp compensation: (a) Circuit diagram; (b) Steady-state waveforms in the CCM.

comparator, compensation ramp with slope m_c and error amplifier. The voltage v_S across sensing resistor is given by $i_{S1}R_s$, where i_{S1} is the switch current.

Fig. 1(b) shows operation waveforms of a PCM controlled flyback converter with ramp compensation when the magnetic inductor operates in the continuous conduction mode (CCM). At the beginning of each switching cycle, the switch S_1 is turned on and the diode S_2 is turned off, which makes the magnetic inductor current i_{Lm} and v_S increase linearly from their initial values. When v_S increases to the control signal v_{con}, S_1 is turned off, and S_2 is turned on, which makes i_{Lm} and v_S decrease linearly until the end of the present switching cycle.

B. Sampled-Data Modeling

From Fig. 1(b), it is found that there are two operation states in the CCM: State 1: S_1 is turned on and S_2 is turned off; State 2: S_1 is turned off and S_2 is turned on. From the aforementioned operation principles, the magnetic inductor is charged and the output capacitor is supplied to the load separately in State 1. The corresponding equivalent circuit is

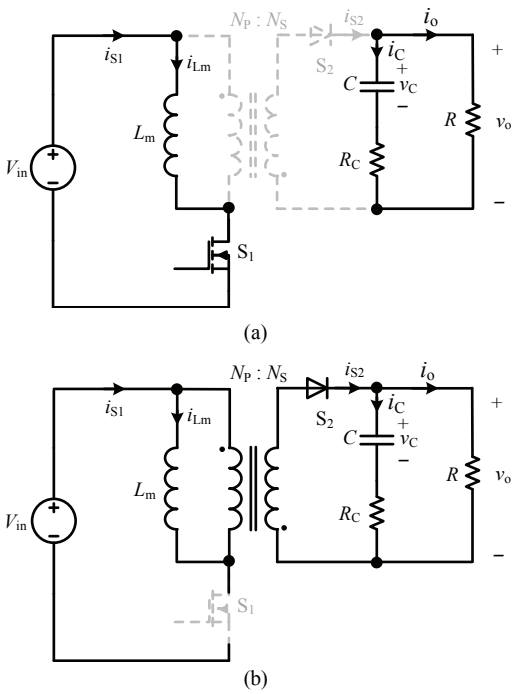

Fig. 2. Equivalent circuits of a CCM flyback converter: (a) State 1: S_1 ON, S_2 OFF; (b) State 2: S_1 OFF, S_2 ON.

shown in Fig. 2(a).

To investigate the dynamics of a PCM controlled flyback converter, a special sampled-data modeling is performed by assuming that the increasing and decreasing slopes of i_{Lm} are constant during each switching cycle, which are given as $m_1 = V_{in}/L$, $m_2 = V_o/(NL)$, respectively, where V_o is the DC output voltage and $N = N_P/N_S$. The output voltage ripple is neglected here because of its trivial influence on the slopes of i_{Lm}. The state equation of Fig. 2(a) are obtained as:

$$L_m \frac{di_{Lm}}{dt} = V_{in} \tag{1a}$$

$$C\frac{dv_C}{dt} = -i_o \tag{1b}$$

Thus, at the instant of the switch S_1 being turned off, i_{Lm} and the output capacitor voltage v_C are easily given by:

$$i_{Lm}(n+d) = i_{Lm}(n) + m_1 t_{on} \tag{2a}$$

$$v_C(n+d) = v_C(n) - \frac{i_o}{C} t_{on} \tag{2b}$$

where $i_{Lm}(n)$ and $v_C(n)$ are the initial values of i_{Lm} and v_C at the beginning of the n-th switching cycle.

In State 2, the magnetic inductor is discharged and i_{Lm} decreases linearly, the load is supplied by both the magnetic inductor and the output capacitor, and the corresponding equivalent circuit is shown in Fig. 2(b). The state equation of Fig. 2(b) can be obtained as:

$$L_m \frac{di_{Lm}}{dt} = -\frac{V_o}{N} \tag{3a}$$

$$C\frac{dv_C}{dt} = Ni_{Lm} - i_o \tag{3b}$$

Similarly, i_{Lm} and v_C at the end of the n-th switching cycle can be expressed as:

$$i_{Lm}(n+1) = i_{Lm}(n+d) - m_2 t_{off} \tag{4a}$$

$$v_C(n+1) = v_C(n+d) + \frac{Ni_{Lm}(n+d) - i_o}{C} t_{off} - \frac{Nm_2}{2C} {t_{off}}^2 \tag{4b}$$

From Eq. (2) and Eq. (4), i_{Lm} and v_C at the beginning of the (n+1)th switching cycle for the CCM flyback converter can be rewritten as follows:

$$i_{Lm}(n+1) = i_{Lm}(n) + (m_1 + m_2)t_{on} - m_2 T_s \tag{5a}$$

$$\begin{aligned} v_C(n+1) = {} & v_C(n) - \frac{i_o}{C} t_{on} - \frac{Nm_2(T_s - t_{on})^2}{2C} \\ & + \frac{N[i_{Lm}(n) + m_1 t_{on}] - i_o}{C}(T_s - t_{on}) \end{aligned} \tag{5b}$$

From Fig. 1(b), when the converter shifts State 1 into State 2, the voltage v_s of the inner loop is equal to the control voltage v_{con} of the outer loop. Meanwhile from Fig. 1(a), v_s and v_{con} meet the equations below:

$$v_s = \begin{bmatrix} R_s & 0 \end{bmatrix} \mathbf{x} \tag{6a}$$

$$v_{con} = k_p \left\{ V_{ref} - k_v \left[v_C(n+d) + i_o R_C \right] \right\} - m_c t_{on} \tag{6b}$$

where $\mathbf{x} = [i_{Lm}, v_C]^T$, T represents the transposed matrix, k_p is the proportional coefficient of the error amplifier, k_v is the sampling coefficient of the output voltage, and m_c is the slope of the compensation ramp. Therefore, the control constraint can be expressed as follows:

$$s_1(\mathbf{x}, t_{on}) = v_s - v_{con} = 0 \tag{7}$$

Eqns. (5) - (7) constitute the sampled-data model of a PCM controlled flyback converter. Based on this, the dynamic analysis of converter can be performed effectively.

III. Dynamic Analysis

A. Bifurcation Behaviors

When the circuit parameters V_{in} = 12V, V_{ref} = 2V, L_m = 100μH, R_C = 50mΩ, R = 4Ω, N_p : N_s = 1:1, k_p = 6, k_v = 0.5 and T_s = 20μs are keep constant, while C varies from 47μF to 100μF, bifurcation diagrams of i_{Lm} and the output voltage v_o of a PCM controlled flyback converter without compensation, *i.e.* m_c = 0, are obtained and shown in Fig. 3(a) and Fig. 3(b), respectively. Similarly, by introducing a compensation ramp with m_c = 5000V/s, bifurcation diagrams are obtained as shown in Fig. 4(a) and Fig. 4(b).

From Fig. 3, it is found that the PCM controlled flyback converter operates in stable period-1 state when C = 100μF. As C decreases, the orbit of the converter is transferred from steady period-1 state to subharmonic oscillation (period-2

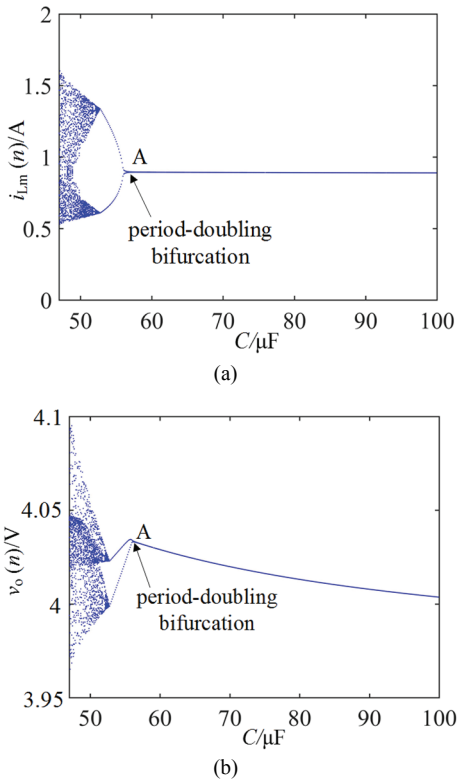

Fig. 3. Bifurcation diagrams of a PCM controlled flyback converter with C varying ($m_c = 0$): (a) i_{Lm}; (b) v_o.

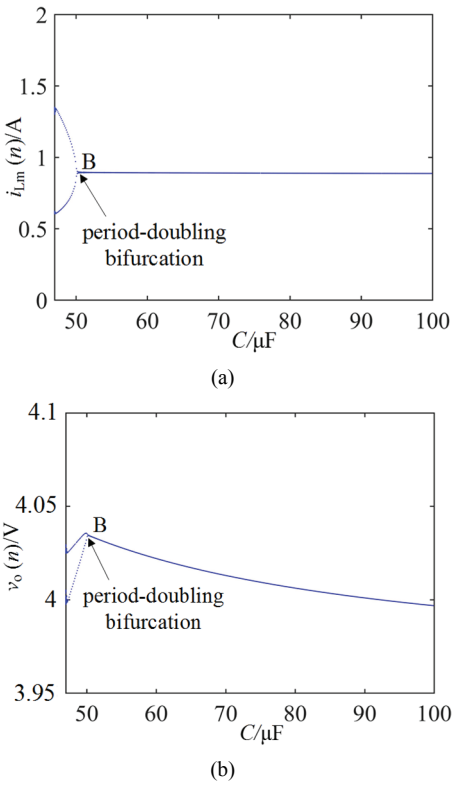

Fig. 4. Bifurcation diagrams of PCM controlled flyback converter with C varying ($m_c = 5000$V/s): (a) i_{Lm}; (b) v_o.

state) owing to the period-doubling bifurcation at $C = 56$μF, *i.e.* at point A shown in Fig. 3. When the parameter C decreases to 52.6μF, a CCM chaotic orbit appears. As observed from Fig. 3, when the parameter C gradually decreases, the PCM controlled flyback converter has a route of CCM period-1, period-doubling bifurcation, CCM period-2 and CCM chaotic state, which means that the converter is more stable with a larger capacitor C. However, in practical applications, the capacitance of the output capacitor C should be small to reduce the size and cost of the converter. Therefore, a compromise exists in choosing the value of the output capacitor C.

As observed from Fig. 4, period-doubling bifurcation occurs at point B when $C = 50$μF and $m_c = 5000$V/s. Comparing Fig. 4 with Fig. 3, it can be seen that the point of period-doubling bifurcation moves left and that the region of stable CCM period-1 becomes wider. This indicates that the system stable range can be widened by ramp compensation.

The bifurcation behavior can be analyzed in a similar way when k_p is taken as a bifurcation parameter. By fixing $C = 100$μF and $m_c = 0$, bifurcation diagrams can be obtained and are shown in Fig. 5 with k_p changing from 1 to 12. It can be observed that with an increase of k_p, period-doubling bifurcation occurs at point C when $k_p = 10.5$, which makes a period-2 orbit develop. With a further increase of k_p, the converter enters into a CCM chaotic state at $k_p = 11.3$. In the design of the control circuit parameters, a faster transient

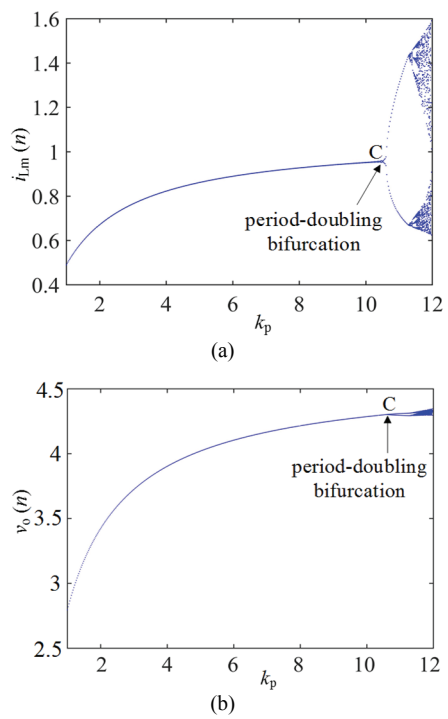

Fig. 5. Bifurcation diagrams of a PCM controlled flyback converter with k_p varying in relation to: (a) i_{Lm}; (b) v_o.

response is obtained with a larger proportional coefficient k_p of the error amplifier. Therefore, engineering designers tend to choose a larger k_p to improve the response speed of the

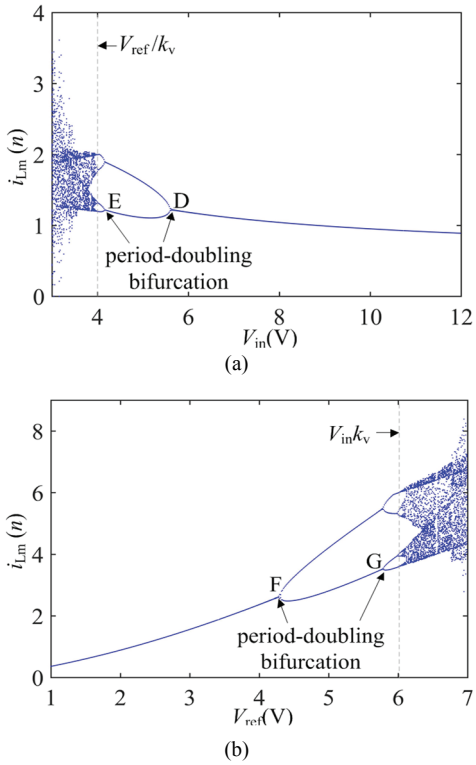

Fig. 6. Bifurcation diagrams of i_{Lm} for a PCM controlled flyback converter with V_{in} and V_{ref} varying in relation to: (a) V_{in}; (b) V_{ref}.

converter. However, in the analysis of Fig. 5, the larger the value of k_p, the more unstable the converters become. In addition, a smaller k_p makes the converters operate in the stable state easily. However, this leads to a large steady state error and a slow response. Hence, it is of great importance to select a proper k_p to achieve the stability and response speed of the system.

Fig. 6(a) and Fig. 6(b) show bifurcation diagrams for a flyback converter under variations of V_{in} = 3 ~ 12V and V_{ref} = 1 ~ 7V, respectively. With a decrease of V_{in}, the orbit of the flyback converter enters into period-2 state from CCM period-1 state, due to the first period-doubling bifurcation at point D where V_{in} = 5.6V. When V_{in} gradually decreases, the converter enters into CCM period-4 state due to the second period-doubling bifurcation at point E, where V_{in} = 4.2V. When V_{in} decreases to 4V, *i.e.* $V_{in} = V_{ref}/k_v$ = 4V, the converter operates in CCM chaotic state. Similarly, as observed from Fig. 6(b), when the parameter V_{ref} gradually decreases, the flyback converter experiences an opposite bifurcation behavior with V_{in} decreasing. Its first and second period-doubling bifurcations occur at point F and point G, respectively, where V_{ref} = 4.3V and 5.8V. When $V_{ref} = V_{in}k_v$ = 6V, the orbit of the converter is transformed from CCM period state to CCM chaotic state. From the above analysis, it is found that the PCM controlled flyback converter operates in CCM chaotic state when the output voltage is larger than or equal to the input voltage, *i.e.* $D \geq 0.5$. This means that the duty range is $D < 0.5$ when the flyback converter operates in stable state.

B. Maximal Lyapunov Exponent

The maximal Lyapunov exponent can be used to represent the characteristics of system movement [4], [7]. When the maximal Lyapunov exponent is smaller than 0, the system is in periodic orbit. Otherwise, the system is in chaotic state. The period-doubling bifurcation occurs when the maximal Lyapunov exponent reaches zero from negative and then goes back to negative. Therefore, the correctness of the sampled-data model for a PCM controlled flyback converter can be verified by investigating the maximal Lyapunov exponent.

The Newton-Raphson method or other numerical algorithms can be used to solve the fixed point $\mathbf{X}_Q = [I_{Lm}\ V_C]^T$ by putting $\mathbf{x}_{n+1} = \mathbf{x}_n = \mathbf{X}_Q$. The Jacobian of the sampled-data model of the PCM controlled flyback converter around the fixed point $\mathbf{X}_Q$ is given by:

$$\mathbf{J}_n(\mathbf{X}_Q) = \begin{bmatrix} J_{11} & J_{12} \\ J_{21} & J_{22} \end{bmatrix}\Bigg|_{\mathbf{x}_n=\mathbf{X}_Q} \tag{8}$$

where:

$$J_{11} = \partial i_{Lm}(n+1)/\partial i_{Lm}(n),\quad J_{12} = \partial i_{Lm}(n+1)/\partial v_C(n),$$
$$J_{21} = \partial v_C(n+1)/\partial i_{Lm}(n),\quad J_{22} = \partial v_C(n+1)/\partial v_C(n).$$

According to Eqns. (1) ~ (7), the following is obtained:

$$J_{11} = 1 - \frac{CR_s(m_2+m_1)}{\Delta},\quad J_{12} = -\frac{C(m_2+m_1)k_p}{\Delta},$$
$$J_{21} = \frac{N}{C}(T_s - t_{on}) - \frac{N(m_2+m_1)T_s - Ni_L(n) - N(2m_1+m_2)t_{on}}{\Delta}R_s,$$
$$J_{22} = 1 - \frac{N(m_2+m_1)T_s - Ni_L(n) - N(2m_1+m_2)t_{on}}{\Delta}k_p,$$

where $\Delta = R_s m_1 C + m_c C - k_p I_o$.

The characteristic equation of Eq. (8) is:

$$\det\left[\lambda\mathbf{1} - \mathbf{J}_n(\mathbf{X}_Q)\right] = 0 \tag{9}$$

The two eigenvalues λ1 and λ2 of the system can be obtained from Eq. (9).

The two Lyapunov exponents of the two-dimensional system are represented as [4]:

$$\begin{bmatrix} \lambda_1 \\ \lambda_2 \end{bmatrix} = \lim_{n\to\infty}\frac{1}{n}\ln\left|\mathrm{eig}(\mathbf{J}_n\mathbf{J}_{n-1}\cdots\mathbf{J}_1)\right| \tag{10}$$

In addition, the maximal Lyapunov exponent is given by:

$$\lambda_{max} = \max\{\lambda_1, \lambda_2\} \tag{11}$$

where eig($\mathbf{J}_n$ $\mathbf{J}_{n-1}$…$\mathbf{J}_1$) is the function to obtain the eigenvalues of ($\mathbf{J}_n$ $\mathbf{J}_{n-1}$…$\mathbf{J}_1$) and max(λ_1, λ_2) is the function to acquire the maximal value between λ_1 and λ_2.

By using Eqns. (8) ~ (11), the maximal Lyapunov exponent spectra corresponding to Fig. 3 and Fig. 4 are shown in Fig. 7(a) and Fig. 7(b), respectively. From Fig. 7(a), when C decreases without ramp compensation, the maximal Lyapunov

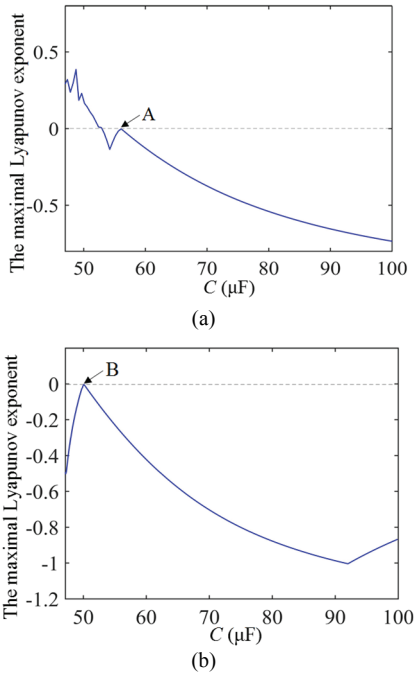

Fig. 7. Lyapunov exponent spectra of a PCM controlled flyback converter with C varying in relation to: (a) m_c = 0; (b) m_c = 5000V/s.

exponent reaches zero from the negative at point A, where C = 56μF. This means that the converter undergoes period-doubling bifurcation, corresponding to point A of the bifurcation diagram shown in Fig. 3. Meanwhile, at C = 52.6μF, the maximal Lyapunov exponent changes from the negative to the positive, which means that the flyback converter enters into chaotic state.

Comparing Fig. 7(a) with Fig. 7(b), the period-doubling bifurcation occurs at C = 50μF after introducing the ramp compensation. This indicates that the point of the Lyapunov exponent reaches zero from the negative and goes back to the negative as it moves left. From the above analysis, it is known that the maximal Lyapunov exponent spectra verifies the correctness of the bifurcation diagrams.

IV. Boundary Equations and Operating-State Regions

A. Boundary Equations

To ensure stable operation, all of the eigenvalues of the Jacobian evaluated at the fixed point are inside a unit circle, i.e. $1 \geq \lambda \geq -1$. In particular, the first period-doubling occurs when λ = -1 [7]. Hence, by putting λ = -1, the stability boundary equation of a PCM controlled flyback converter is obtained as:

$$\det\left[\lambda \mathbf{1} - \mathbf{J}_n(\boldsymbol{X}_Q)\right]\Big|_{\lambda=-1} = 0 \tag{12}$$

From Fig. 1, the valley magnetic inductor current i_n, the increasing slope m_1 and the decreasing slope m_2 are satisfied as:

$$i_n = \frac{i_o}{D} - \frac{1}{2} m_1 t_{on}, \quad \frac{m_2}{m_1} = \frac{D}{1-D} = \frac{v_o}{NV_{in}} \tag{13}$$

where the duty ratio $D = t_{on}/T_s$. By substituting Eq. (13) into Eq. (12), the simplified stability boundary from stable period-1 state to subharmonic oscillation state can be yielded as:

$$\begin{aligned} &4m_c C(1-D) - k_p(1-D)\left(m_1 T_s(N(1-2D)+D) + 4i_o\right) \\ &+2\left(m_1 R_s C(1-D-\frac{D}{N}) - Nk_p i_o\right) = 0 \end{aligned} \tag{14}$$

Eq. (14) indicates that whether the PCM controlled flyback converter is stable or not depends on all of the circuit parameters. If the left of Eq. (14) is less than 0, the flyback converter operates in period-1 state, otherwise it operates in unstable state.

B. Operation-State Regions

In order to verify the correctness of the stability boundary equation of a PCM controlled flyback converter, the divisions of the operation-state regions are drawn utilizing Eq. (14) with C and k_p varying under different value of V_{in} and V_{ref}, as shown in Fig. 8 and Fig. 9 respectively. Here, the blue solid lines represent the stability boundary equation without ramp compensation and the red doted lines stand for the equation with ramp compensation.

Considering that the variation ranges of the circuit parameters are V_{in} = 3 ~ 12V and C = 47 ~ 100μF, and that the other circuit parameters are chosen to be the same as those in Fig. 3, the operation-state regions of V_{in} and C can be obtained in Fig. 8(a). This shows that there are two operation-state regions, i.e., the stable region and the unstable region, which are divided by boundary equations. With V_{in} increasing, the stable operation state of a flyback converter without ramp compensation is widened. Meanwhile, the system stability region is enlarged by increasing C. This indicates that the stable operation-state region of the flyback converter can be broadened by increasing V_{in} or by increasing C. In addition, the converter's stable period-1 operation region becomes wider by introducing ramp compensation (m_c = 5000V/s). By choosing a vertical line with V_{in} = 12V, as shown in Fig. 8(a), the bifurcation process is obtained when C varies, which corresponds to Fig. 3. The critical instability points of the flyback converters without compensation and with compensation in Fig. 8(a) correspond to point A and point B, respectively. This is consistent with the first period-doubling bifurcation points in Fig. 3 and Fig. 4. Similarly, the bifurcation process while V_{in} varies is obtained via a horizontal line with C = 100μF, as shown in Fig. 8(a). The corresponding bifurcation diagrams are observed from Fig. 6. Point D and point E, corresponding to the first and the second period-doubling bifurcation points without ramp compensation in Fig. 6(a), are in the stable region and unstable region shown in Fig. 8(a). After introducing ramp compensation, the second period-doubling bifurcation point

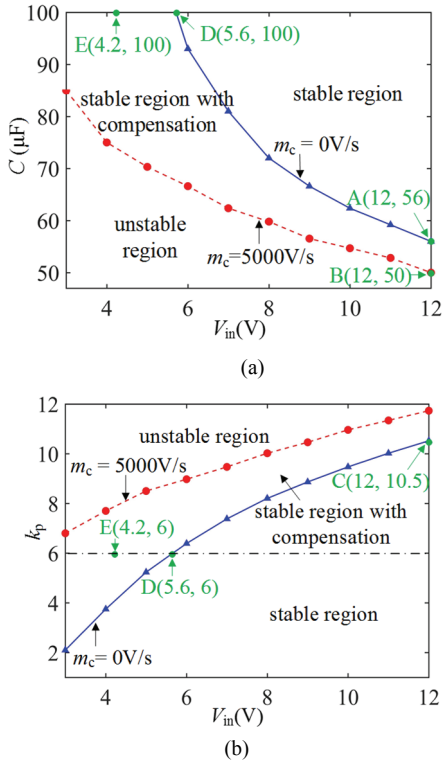

Fig. 8. Operation-state regions for C and k_p with variation of V_{in}: (a) V_{in} - C; (b) V_{in} - k_p.

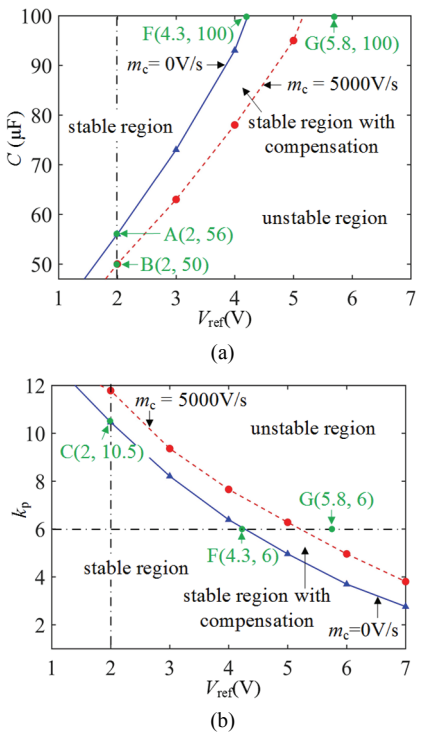

Fig. 9. Operation-state regions about C and k_p with variations of V_{ref}: (a) V_{ref} - C; (b) V_{ref} - k_p.

D shifts into the stable region from the unstable region.

Fig. 8(b) shows the operation-state regions of V_{in} and k_p by fixing C = 100μF. When V_{in} is constant, the stable operation range is broadened with k_p gradually decreasing. In addition, the first period-doubling bifurcation point C in Fig. 5, is located in the stability boundary line shown in Fig. 8(b).

Setting V_{in} = 12V, choose: a) V_{ref} = 1 ~ 7V, C = 47 ~ 100μF; b) V_{ref} = 1 ~ 7V, k_p = 1 ~ 12, and the other circuit parameters are chosen to be the same as those used for Fig. 3. Then the operation-state regions of the flyback converter can be obtained according to Eq. (14), as shown in Fig. 9(a) and Fig. 9(b), respectively. As observed from Fig. 9, a reduction of V_{ref} broadens the stable operation range with a constant C. When V_{ref} is fixed, by increasing C, decreasing k_p, or introducing a ramp compensation can control the flyback converter to operate in the stable CCM period-1 state. This provides helpful guidance to effectively estimate the circuit parameters range, for the PCM controlled flyback converter operating in the stable period-1 state.

From the above analysis, the duty ratio range for the flyback converter without compensation operating in the stable period-1 state is D < 0.5. In addition, the stability regions in the parameter space between the output capacitor and the proportional coefficient of the error amplifier are enlarged by increasing the input voltage or by decreasing the reference voltage. Furthermore, the stable operation range of the converter is effectively improved after introducing ramp compensation.

V. Simulation and Experimental Results

A. Simulation Waveforms

In order to verify the correctness of the theoretical analysis, the circuit parameters are the same as those used for the bifurcation diagram shown in Fig. 3, and the circuit is simulated by PSIM software. Then time-domain simulation waveforms of a PCM controlled flyback converter are obtained under different circuit parameters, as shown in Fig. 10.

The critical value of the capacitor is calculated to be equal to 56μF by taking the simulation parameters into Eq. (14) in a PCM controlled flyback converter without ramp compensation. When C = 57μF (> 56μF), the value on the left of Eq. (14) is greater than zero and the converter operates in the stable CCM period-1 state shown in Fig. 10(a), where V_{in} = 12V, V_{ref} = 2V, k_p = 6 and C = 57μF. Reducing the capacitance to 50μF, the flyback converter operates in the unstable state, as shown in Fig 10(b), which coincides with the result of point B shown in Fig. 8 and Fig. 9 without ramp compensation. By substituting C = 50μF into Eq. (14), the critical value of the slope m_c = 5000V/s is required. When C = 51μF (> 50 F) and m_c = 5000V/s, the value on the left of Eq. (14) is greater than zero, and the converter enters the steady state, as shown in Fig. 10(c).

Fixing C = 100μF, the converter presents the unstable state when the reference voltage V_{ref} increases to 5V, while the converter operates in the stable period-1 state by introducing

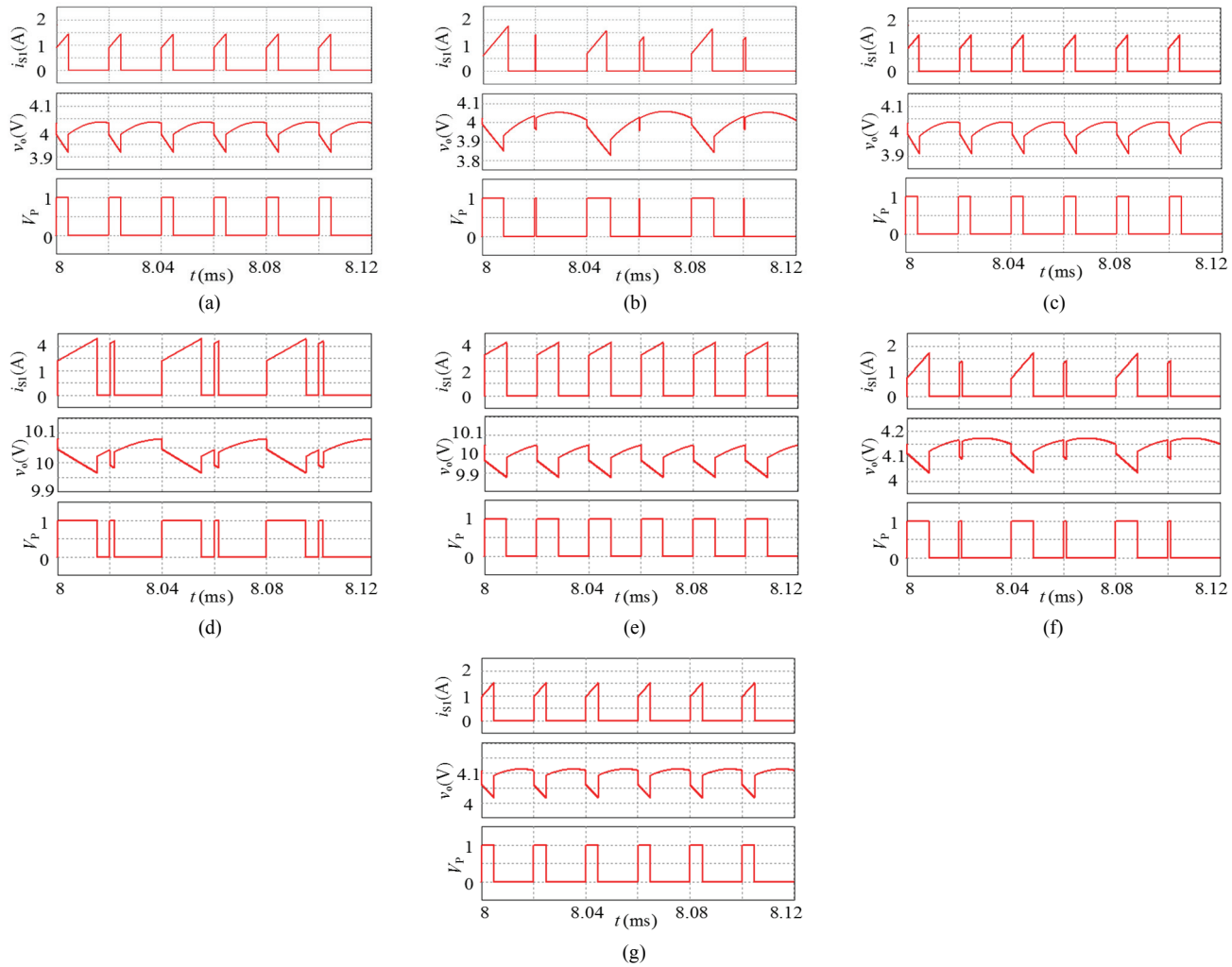

Fig. 10. Time-domain simulation waveforms: (a) V_{ref} = 2V, k_p = 6, C = 57μF, m_c = 0; (b) V_{ref} = 2V, k_p = 6, C = 51μF, m_c = 0; (c) V_{ref} = 2V, k_p = 6, C = 51μF, m_c = 5000V/s; (d) V_{ref} = 5V, k_p = 6, C = 100μF, m_c = 0; (e) V_{ref} = 5V, k_p = 6, C = 100μF, m_c = 5000V/s; (f) V_{ref} = 2V, k_p = 11, C = 100μF, m_c = 0; (g) V_{ref} = 2V, k_p = 11, C = 100μF, m_c = 5000V/s.

a compensation ramp with a slope of m_c = 5000V/s, where the corresponding time-domain simulation waveforms are shown in Fig. 10(d) and Fig. 10(e), respectively.

By increasing k_p from 6 to 11, it is observed in Fig. 10(a) and Fig. 10(f) that the converter enters from the stable state into the unstable state. After introducing m_c = 5000V/s, the converter returns to the stable state.

Therefore, it can be concluded that the larger output capacitor, smaller reference voltage and smaller proportional coefficient can make the converter more stable. Moreover, the ramp compensation can make the flyback converter shift from the unstable state to the stable state. The simulation results shown in Fig. 10 are consistent with the operation-state regions in Fig. 8 and Fig. 9. Then the correctness of the theoretical analysis is verified.

B. Experimental Verification

To verify the validity of the simulation results, experimental studies of a PCM controlled flyback converter with ramp compensation are performed with the same circuit parameters as the simulation circuit. A photograph of the experimental set-up is shown in Fig. 11, where the switch S_1 is an N-channel power MOSFET (IRF740), the switch S_2 is a diode (MUR10120), the driver is a UCC27517, and the PWM

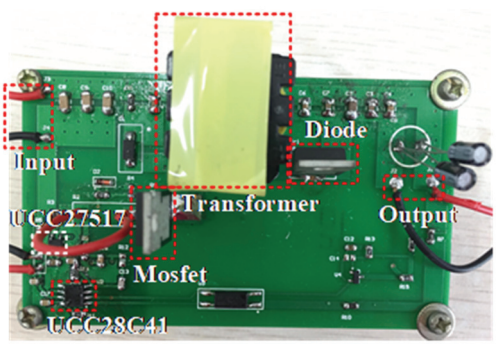

Fig. 11. Photograph of the experimental setup.

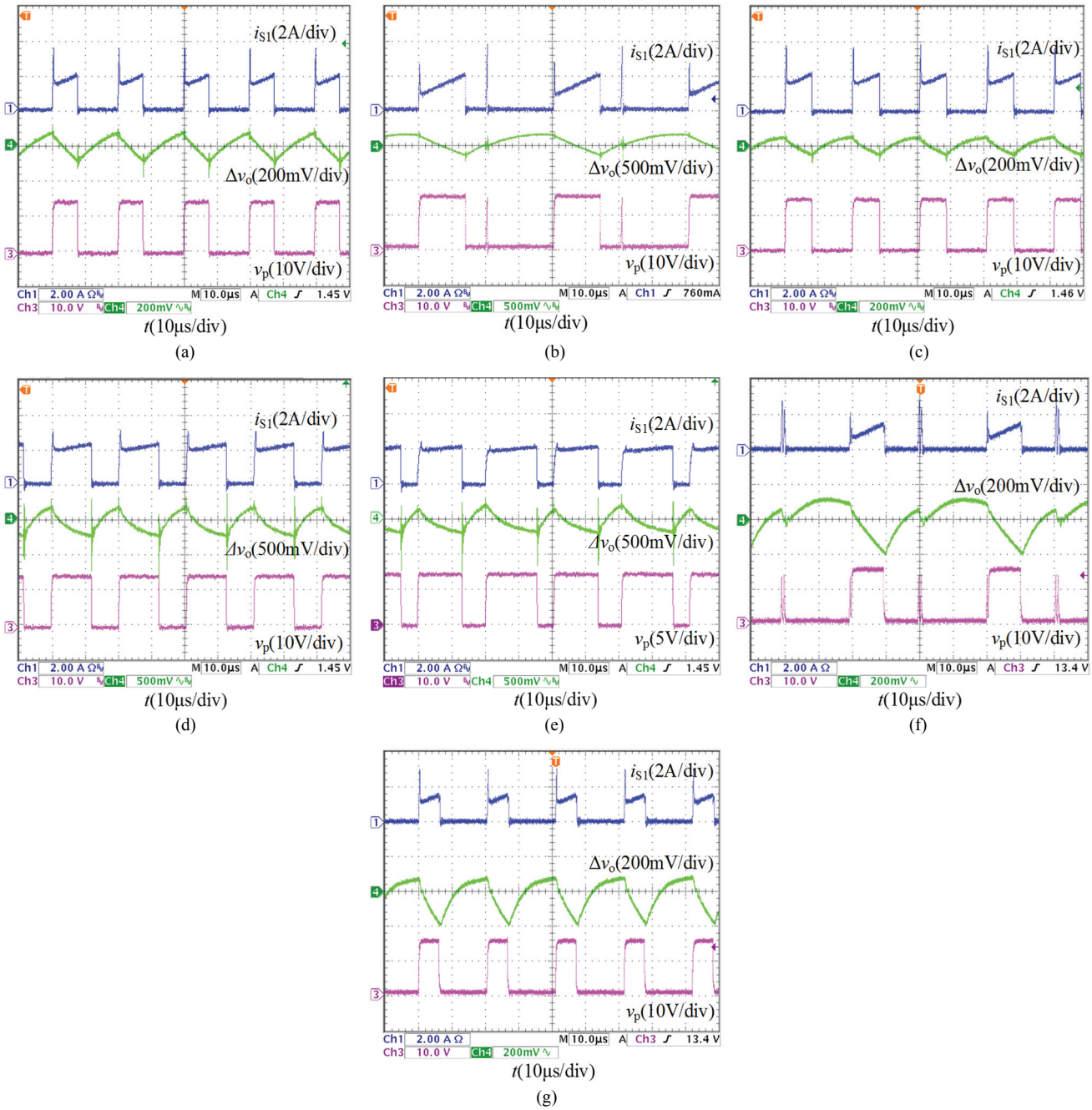

Fig. 12. Experimental waveforms: (a) V_{ref} = 2V, k_p = 6, C = 57μF, m_c = 0; (b) V_{ref} = 2V, k_p = 6, C = 51μF, m_c = 0; (c) V_{ref} = 2V, k_p = 6, C = 51μF, m_c = 5000V/s; (d) V_{ref} = 5V, k_p = 6, C = 100μF, m_c = 0; (e) V_{ref} = 5V, k_p = 6, C = 100μF, m_c = 5000V/s; (f) V_{ref} = 2V, k_p = 11, C = 100μF, m_c = 0; (g) V_{ref} = 2V, k_p = 11, C = 100μF, m_c = 5000V/s.

signal is generated by a UCC28C41PCM controller. Waveforms of the switching current i_{S1}, output voltage ripple Δv_o, and driving signal v_p are obtained under different circuit parameters, as shown in Figs. 12(a)-(g).

As can be seen from Fig. 12, when C = 57μF, the PCM controlled flyback converter operates in the CCM period-1 state, shown as Fig. 12(a). When C = 51μF, the converter operates in the unstable state, shown as Fig. 12(b). However, when C = 51μF, by introducing a compensation ramp with m_c = 5000V/s, the converter operates in the CCM period-1 state, as shown in Fig. 12(c). In Fig. 12(d), the converter is in the unstable state while V_{ref} = 5V. When k_p = 11, the converter undergoes the unstable state in Fig. 12(f). When m_c = 5000V/s, the operation mode of the converter shifts from the unstable state to the stable CCM period-1 state, as shown in Fig. 12(e) and Fig. 12(g). These experimental waveforms are consistent with the time domain simulation waveforms shown in Fig. 10, which verifies the correctness of the simulation results.

VI. CONCLUSIONS

In this paper, the operation principle of a PCM controlled flyback converter is studied first. Then a dynamic model where the magnetic inductor current operates in the CCM is established, utilizing sampled-data modeling method. Based on this, the bifurcation diagrams and Lyapunov exponent spectrum with parameters variation are analyzed, including the output capacitor, proportional coefficient of the error amplifier, input voltage and reference voltage. In addition, the stability boundary equation of the PCM controlled flyback converter with compensation is derived from the characteristic equation of a Jacobian matrix. Based on this, the operation- state regions under variations of the output capacitor and proportional coefficient with different input and reference voltages are obtained. Finally, circuit simulation and experimental results are provided to verify the correctness of the theoretical analysis. The research results indicate several things.

i) A larger output capacitor and input voltage, and a smaller proportional coefficient and reference voltage, can make the converter more stable.

ii) The duty ratio range when a PCM controlled flyback converter operates in the stable state is $D < 0.5$. In addition, the stability regions in the parameter space between the output capacitor and the proportional coefficient of the error amplifier are enlarged by increasing the input voltage or by decreasing the reference voltage.

iii) By introducing ramp compensation, the stable operation range of a PCM controlled flyback converter can be effectively broadened.

ACKNOWLEDGMENT

This work was supported by the National Natural Science Foundation of China (61771405 and 61371033), the Innovation Research Team of Youth Science and Technology in Sichuan Province (19CXTD0007), the Fund of Chengdu Science and Technology Bureau (2016-HM01-00139-SF), and the Cultivation Project of Excellent Doctorate Dissertation of Southwest Jiaotong University of China.

REFERENCES

[1] J. H. B. Deane and D. C. Hamill, "Instability, subharmonics, and chaos in power electronic systems," *IEEE Trans. Power Electron.*, Vol. 5, No. 3, pp. 260-268, Jul. 1990.

[2] A. E. Aroudi, M. Orabi, R. Haroun, and L. Martinez-Salamero, "Asymptotic slow-scale stability boundary of PFC AC-DC power converters: Theoretical prediction and experimental validation," *IEEE Trans. Power Electron.*, Vol. 58, No. 8, pp. 3448-3460, Nov. 2010.

[3] F. Q. Wang, H. Zhang, and X. Ma, "Period-doubling bifurcation in two-stage power factor correction converters using the method of incremental harmonic balance and Floquet theory," *Chin. Phys. B*, Vol. 21, No. 2, pp. 050501-050510, Jan. 2012.

[4] J. P. Wang, B. C. Bao, J. P. Xu, G. H. Zhou, and W. Hu, "Dynamical effects of equivalent series resistance of output capacitor in constant on-time controlled Buck converter," *IEEE Trans. Ind. Electron.*, Vol. 60, No. 5, pp. 1759-1768, May 2013.

[5] J. D. Morcillo, D. Burbano, and F. Angulo, "Adaptive ramp technique for controlling chaos and sub-harmonic oscillations in DC-DC power converters," *IEEE Trans. Power Electron.*, Vol. 31, No. 7, pp. 5330-5343, Jul. 2016.

[6] B. C. Bao, G. H. Zhou, J. P. Xu, and Z. Liu, "Unified classification of operation-state regions for switching converters with ramp compensation," *IEEE Trans. Power Electron.*, Vol. 26, No. 7, pp. 1968-1975, Jul. 2011.

[7] S. H. Zhou, G. H. Zhou, Y. Wang, X. T. Liu, and S. G. Xu, "Bifurcation analysis and operation region estimation of current-mode-controlled SIDO boost converter," *IET Power Electron.*, Vol. 10, No. 7, pp. 846-853, Jun. 2017.

[8] H. Zhang, D. Y. Chen, C. Z. Wu, and X. Y. Wang, "Dynamics analysis of the fast-slow hydro-turbine governing system with different time-scale coupling," *Communications in Nonlinear Science and Numerical Simulation*, Vol. 54, pp. 136-147, Jan. 2018.

[9] E. Rodriguez, A. E. Aroudi, F. Guinjoan, and E. Alarcon, "A ripple-based design-oriented approach for predicting fast-scale instability in DC–DC switching power supplies," *IEEE Trans. Circuits Syst. I, Reg. Papers*, Vol. 59, No. 1, pp. 215-227, Jan. 2012.

[10] Y. F. Chen, C. K. Tse, S. S. Qiu, L. Lindenmuller, and W. Schwarz, "Coexisting fast-scale and slow-scale instability in current-mode controlled DC-DC converters analysis, simulation and experimental results," *IEEE Trans. Circuits Syst. I, Reg. Papers*, Vol. 55, No. 10, pp. 3335-3348, Nov. 2008.

[11] G. H. Zhou, B. C. Bao, and J. P. Xu, "Complex dynamics and fast-slow scale instability in current-mode controlled buck converter with constant current load," *Int. J. Bifurc. Chaos*, Vol. 23, No. 4, 1350062, Apr. 2013.

[12] Q. Wu and Z. M. Zhu, "A versatile OCP control scheme for discontinuous conduction mode flyback AC/DC converters," *IEEE Trans. Ind. Electron.*, Vol. 64, No. 8, pp. 6443-6452, Aug. 2017.

[13] Z. M. Zhu, Q. Wu, and Z. Y. Wang, "Self-compensating OCP control scheme for primary-side controlled flyback AC/DC converters," *IEEE Trans. Power Electron.*, Vol. 31, No. 5, pp. 3673-3682, May 2017.

[14] S. Y. Chen, "Small-signal model for a flyback converter with peak current mode control," *IET Power Electron.*, Vol. 7, No. 4, pp. 805-810, Apr. 2014.

[15] J. M. Zhang, X. C. Huang, and X. K. Wu, "A high efficiency flyback converter with new active clamp technique," *IEEE Trans. Power Electron.*, Vol. 25, No. 7, pp. 1775-1785, Jul. 2010.

[16] J. Park, Y. J. Moon, M. G. Jeong, J. G. Kang, S. H. Ki, J. C. Gong, and C. Yoo, "Quasi-resonant (QR) controller with adaptive switching frequency reduction scheme for flyback converter," *IEEE Trans. Ind Electron.*, Vol. 63, No. 6, pp.3571-3581, Feb. 2016.

[17] G. D. Shi, Q. J. Cao, B C Bao, and Z. H. Ma, "Dynamics and operation-state estimation of current-mode controlled flyback converter," *J. Electron. Sci. Technol.*, Vol. 11, No. 3, pp. 306-311, Sep. 2013.

[18] W. F. Qiang and X. K. Ma, "Effects of switching frequency and leakage inductance on slow-scale stability in a voltage

controlled flyback converter," *Chin. Phys. B*, Vol. 22, No. 12, 120504, Dec. 2013.
[19] F. Xie, R. Yang, and B. Zhang, "Bifurcation and border collision analysis of voltage-mode-controlled flyback converter based on total ampere-turns," *IEEE Trans. Circuits Syst. I, Reg. Papers*, Vol. 58, No. 9, pp. 2269-2280, Sep. 2011.
[20] F. H. Hsieh and K. M. Lin, "Chaos phenomenon in UC3842 current-programmed flyback converter," in *The 4th IEEE Conference on Industrial Electronics and Applications (ICIEA)*, pp. 166-171, 2009.

Shuhan Zhou received her B.S. and M.S. degrees in Electronic Engineering from Southwest Jiaotong University, Chengdu, China, in 2014, and 2016, respectively, where she is presently working towards her Ph.D. degree in the School of Electrical Engineering. Her current research interests include modulation and control techniques for high-power density and high-efficiency multiple-output converters, the dynamic modeling and analysis of switching dc-dc converters, and the control techniques of LLC resonant converters.

Guohua Zhou received his B.S. degree in Electronic and Information Engineering and his M.S. and Ph.D. degrees in Electrical Engineering from Southwest Jiaotong University, Chengdu, China, in 2005, 2008 and 2011, respectively. From March 2010 to September 2010, he was a Research Assistant in the Department of Electronic and Information Engineering, Hong Kong Polytechnic University, Kowloon, Hong Kong, China. From October 2010 to March 2011, he was a Visiting Scholar (and a joint Ph.D. student) in the Center for Power Electronics Systems, Virginia Polytechnic Institute and State University, Blacksburg, VA, USA. He is presently working as a Professor in the School of Electrical Engineering, Southwest Jiaotong University. His current research interests include modulation and control techniques of power electronics systems, the dynamic modeling and analysis of switching power converters, and renewable energy applications for power electronics.

Shaohuan Zeng received his B.S. degree in Electronic Engineering from Southwest Jiaotong University, Chengdu, China, in 2016, where he is presently working towards his M.S. degree in the School of Electrical Engineering. His current research interests include the modulation and control techniques of tri-state converters.

Shungang Xu received his M.S. degree in Measurement Technology and Instruments from the University of Electronic Science and Technology of China, Chengdu, China, in 2006; and his Ph.D. degree in Power Electronics and Drives from Southwest Jiaotong University, Chengdu, China, in 2011. Since 2015, he has been with the School of Electrical Engineering, Southwest Jiaotong University. His current research interests include digital control techniques, renewable energy generation, and energy storage systems for electronic vehicles.

Taiqiang Cao received his M.S. degree in Electronics and Communication Engineering from the University of Electronic Science and Technology of China, Chengdu, China, in 2005; and his Ph.D. degree in Power Electronics and Drives from Southwest Jiaotong University, Chengdu, China, in 2010. Since 2011, he has been with School of Electrical Engineering and Electronic Information, Xihua University, Chengdu, China. His current research interests include renewable energy generation, and energy storage systems for electronic vehicles.